Microstructure Development in Finely Atomized Droplets of Copper-Iron Alloys

JIE HE, JIU-ZHOU ZHAO, XIAO-FENG WANG, and LING-LING GAO

The solidification behavior of $Cu_{(100-X)}Fe_X$ (X = 15, 20, 30, and 40) alloys was investigated by gas atomization technology. The effects of the size and composition of the atomized droplet on the microstructure development during cooling through the metastable miscibility gap have been discussed. A smaller atomized droplet achieves a finer dispersed microstructure. Alloys of composition close to the critical composition of the alloy system are relatively easy to undercool into the miscibility gap. The forces acting on the Fe-rich sphere during the liquid-liquid phase transformation were analyzed. The formation of an Fe-poor layer on the powder surface is the result of the common action of the Fe-rich sphere's Marangoni migration and the repulsive interaction between the cellular solid/liquid interface and the solidified Fe-rich sphere. The Fe-rich spheres in the center part of the powder are entrapped between the equiaxed grains of Cu-rich phase and finally distributed at the grain boundaries and triple junctions.

I. INTRODUCTION

ONE of the important techniques of rapid solidification is atomization powder processing. Using this technique, powders are subsequently compacted to obtain the desired shape of an object. The smaller the size of the atomized droplet, the higher the cooling rate is, and the finer the powder microstructure is. By means of the rapid solidification technique, the microstructure of stable or metastable phase can be obtained. The Cu-Fe alloy is well known as a peritectic system.[1] It has a nearly flat liquidus line and a retrograde solidus line and hence displays a thermodynamic tendency toward the formation of a miscibility gap in supercooled liquid state.[2] When a single-phase liquid is undercooled into the metastable miscibility gap, the alloy melt will discompose into two liquids: one is Cu-rich phase (L_1), and the other is Fe-rich phase (L_2), as shown in Figure 1. In order to quantitatively determine the boundary of the metastable miscibility gap, much work has been performed on the thermodynamic calculation,[3,4] and various experiments such as magnetic susceptibility measurement,[2] electromagnetic levitation experiments,[5] and differential thermal analysis[6,7] have been carried out. Although the effect of the cooling rate and undercooling on the liquid-phase decomposition have been investigated,[8,9] thus far little is known about the kinetics of the liquid-liquid phase transformation during cooling in the metastable miscibility gap. Particularly, no literature has been found on the evolution process of the microstructure during the period after the crystallization of the Fe-rich phase prior to the complete solidification of the liquid Cu-rich phase. In the present study, the effect of the volume fraction of the minority phase on the microstructure development is investigated. The Marangoni and gravitational forces acting on the Fe-rich sphere are estimated. The interaction between the solidified Fe-rich sphere and the advancing solid/liquid interface of the Cu-rich phase are discussed in detail. The formation mechanism of the Fe-poor layer on the powder surface is clarified in this article.

JIE HE, Doctoral Candidate, JIU-ZHOU ZHAO, Professor, and XIAO-FENG WANG and LING-LING GAO, Graduate Students, are with Institute of Metal Research, Chinese Academy of Sciences, People's Republic of China. Contact e-mail: jzzhao@imr.ac.cn

Manuscript submitted January 25, 2005.

II. EXPERIMENTAL PROCEDURE

The alloy samples with different compositions shown as four arrows in Figure 1 were prepared by melting high-pure Cu (99.999 at. pct) and Fe (99.99 at. pct) using middle-frequency induction under vacuum. The alloy melt was atomized by high-pressure (2 to 3 MPa) nitrogen gas after the melt temperature reached 1773 K and kept for 20 minutes. The Cu-Fe alloy powders of 20- to 280-μm diameter were obtained. The powders were classified by screening, and were polished and etched for the observation of the microstructure. The microstructure characterization was done using an optical microscope and a scanning electron microscope with energy-dispersive X-ray analysis.

III. RESULTS AND DISCUSSION

A. *Microstructures of Powders of Different Sizes*

The liquidus temperature of the $Cu_{80}Fe_{20}$ alloy is 1670 K. The interval between the liquidus and binodal temperatures amounts to 50 K.[1,4] When the maximum undercooling of the melt is smaller than 50 K, the primary γ-Fe is formed in the parent phase. In other words, the liquid-solid phase transformation takes place. The structures of the powders of various size classifications have been observed by optical microscope. It is indicated that the complete liquid-solid phase transformation takes place in a small quantity of atomized droplets with the largest size classification. This kind of atomized powder has been analyzed by X-ray. It is indicated that the microstructure consists of the primary γ-Fe, the peritectic reaction product ε-Cu, and the eutectoid reaction product α-Fe. Figure 2 shows the stable phase microstructure of a powder of 280-μm diameter. It can be seen that the γ-Fe dendrites distributed arbitrarily in the matrix. The maximum length of the dendritic trunk is 20 μm. A smaller atomized droplet achieves a faster cooling rate

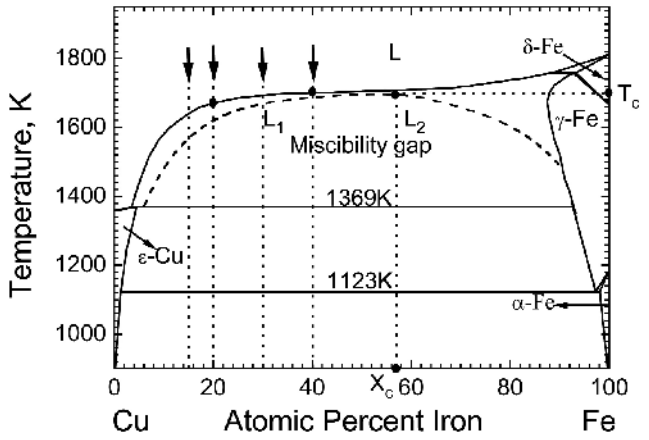

Fig. 1—The phase diagram of Cu-Fe binary alloy. The dashed curve under the liquidus is the binodal line.[4] L_1 and L_2 are Cu-rich and Fe-rich liquid phases, respectively.

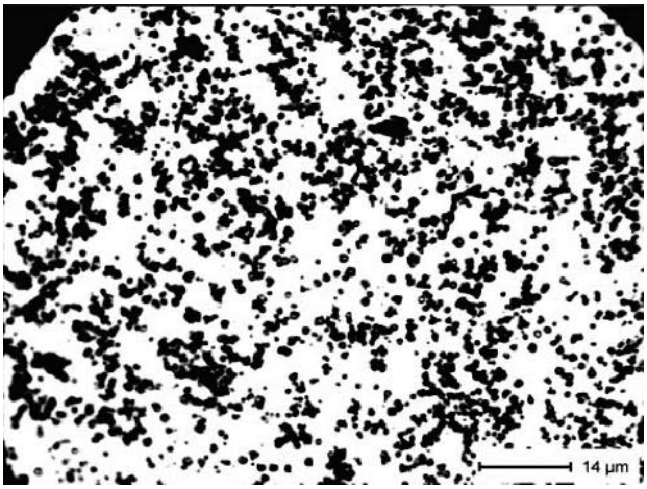

Fig. 3—The microstructure of a $Cu_{80}Fe_{20}$ powder of 100-μm diameter.

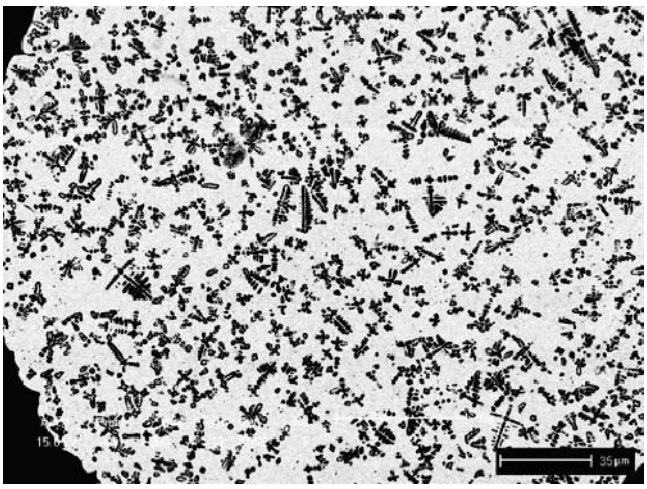

Fig. 2—The microstructure of a $Cu_{80}Fe_{20}$ powder of 280-μm diameter.

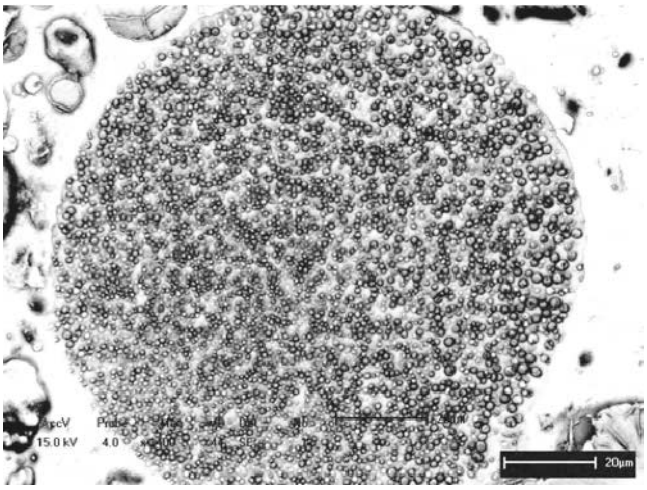

Fig. 4—The microstructure of a $Cu_{60}Fe_{40}$ powder of 100-μm diameter.

and a deeper undercooling.[10] If the single-phase melt reaches a sufficient degree of undercooling, the melt will separate into a Cu-rich phase (L_1) and a Fe-rich phase (L_2). The compositions of the two liquid phases follow the boundary of the miscibility gap during the liquid-liquid phase transformation. The microstructure of a powder of 100-μm diameter is shown in Figure 3. The Fe-rich spheres dispersed in the matrix. The size of the Fe-rich spheres ranges from 0.25 to 1.42 μm. The average diameter is about 0.9 μm. A quantitative metallographic analysis has been conducted for the atomized droplets with different sizes.[11] The results show that the average radius of the minority phase sphere decreases while the number density of the Fe-rich sphere increases with the decrease of the powder size.

B. *Effect of the Alloy Composition*

The liquidus temperature of the $Cu_{60}Fe_{40}$ alloy is 1700 K, and the interval between the liquidus and binodal temperature is about 13 K.[1,4] Compared with the $Cu_{80}Fe_{20}$ alloy, the $Cu_{60}Fe_{40}$ alloy liquid is relatively easy to undercool into the metastable miscibility gap under the same conditions of cooling. The microstructure examinations indicate that $Cu_{60}Fe_{40}$ powders of all sizes consist of Fe-rich spheres and Cu-rich matrix. Figure 4 shows the microstructure of $Cu_{60}Fe_{40}$ powder of 100-μm diameter. One can find by comparing Figures 3 and 4 that the same size powders with different compositions show different microstructures. The size distribution of the Fe-rich spheres in Figure 4 has been determined. It is close to a skew normal distribution according to the fitted result, as shown in Figure 5. The diameter of the Fe-rich spheres ranges from 0.12 to 2.3 μm. The average diameter of Fe-rich spheres in Figure 4 is about 1.2 μm, larger than that of the Fe-rich spheres in Figure 3. The average diameters of the Fe-rich sphere in the same size powders with different alloy compositions were measured. Figure 6 indicates that the average diameter of Fe-rich spheres increases with the increase of Fe concentration in the powders of 100-μm diameter. This is because the vertical interval of the miscibility gap of the alloy is larger when the alloy composition approaches the critical composition X_c, and hence, the Fe-rich sphere has a longer time to grow by diffusion and coarsen by collisions and coagulations between the Fe-rich spheres due to the spheres' motion.

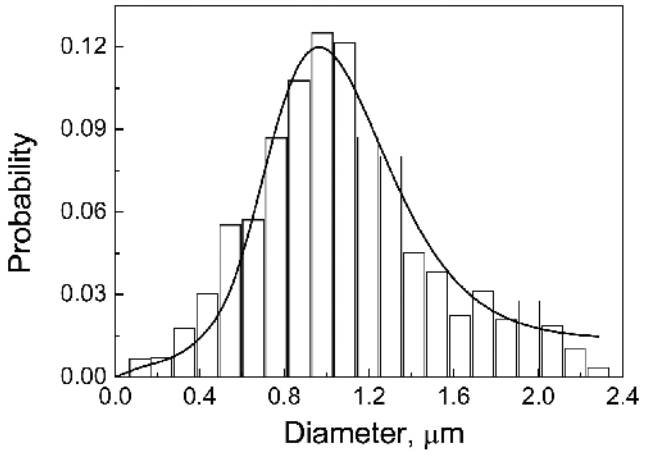

Fig. 5—The size distribution of Fe-rich spheres in the $Cu_{60}Fe_{40}$ powder of 100-μm diameter. The bars and solid curve are the measured and fitted results, respectively.

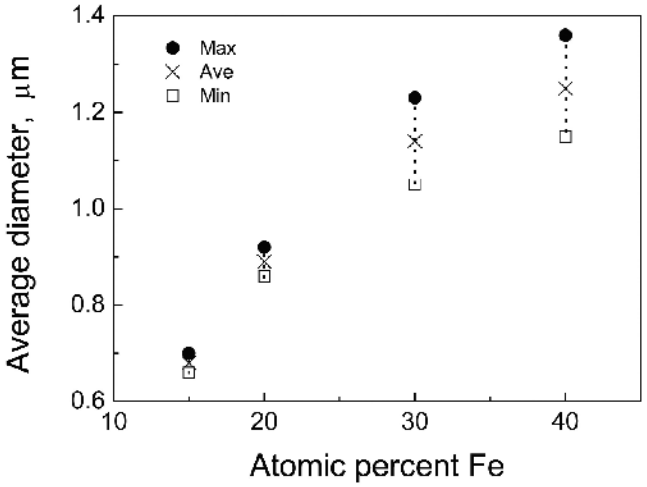

Fig. 6—The average diameters of Fe-rich spheres in 100-μm diameter powders *vs* the Fe concentration.

C. *Forces Acting on the Fe-Rich Sphere*

During cooling of Cu-Fe alloys through the metastable miscibility gap, there exist three characteristic temperatures prior to complete solidification. The first one is the temperature of the onset of the liquid-liquid phase transformation, $T_{L_1L_2}$. Cooling below $T_{L_1L_2}$ results in a continuous liquid-phase decomposition reaction until the Fe-rich phase solidifies at the second characteristic temperature, T_{S_2}. The third one is the temperature at which the Cu-rich liquid phase solidifies completely, T_{S_1}. During cooling in the temperature range from $T_{L_1L_2}$ to T_{S_2}, the minority phase spheres are embedded in the liquid matrix and move due to the Marangoni force and gravitational force. The Marangoni force F_m acting on a single liquid Fe-rich sphere is given by[13,14,15]

$$F_m = -\frac{\pi \eta_m k_m D^2}{(\eta_m + \eta_{L_2})(2k_m + k_{L_2})} \cdot \frac{\partial \sigma}{\partial T} \cdot \nabla T \qquad [1]$$

where k_m and k_{L_2} are the thermal conductivities, and η_m and η_{L_2} are the viscosities of the matrix phase and the minority phase. The term D is the diameter of the minority phase sphere, and σ is the interfacial energy between the liquid matrix and the minority phase.

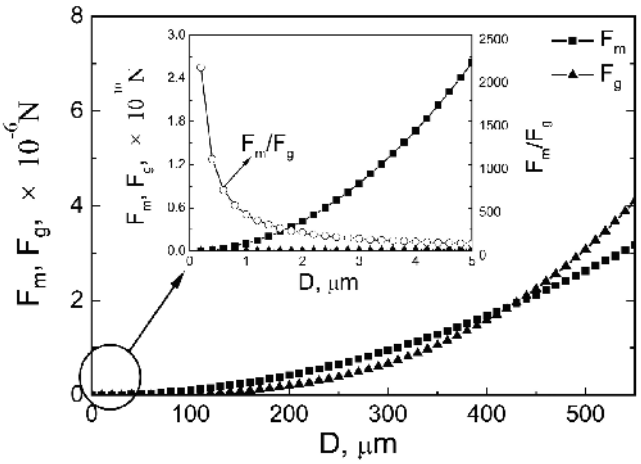

Fig. 7—Marangoni force and gravitational force *vs* the diameter of the Fe-rich sphere.

The interfacial energy between the two liquids can be calculated according to Cahn and Hilliard's model.[16] The value of $\partial\sigma/\partial T$ is given by

$$\frac{\partial \sigma}{\partial T} = -1.26 \cdot \sigma_0 \cdot \frac{1}{T_c} \cdot \left(1 - \frac{T}{T_c}\right)^{0.26} \qquad [2]$$

where $\sigma_0 = 2N_0 \lambda k_B T_c$, with N_0 being the number of atoms per unit volume of liquid, λ the interatomic distance, k_B the Boltzmann's constant, and T_c the critical temperature.

The gravitational force F_g is determined by the gravity level g and the density difference $\Delta\rho$ between the minority phase and the matrix. It is given by

$$F_g = \frac{\pi}{6} D^3 \Delta\rho \cdot g \qquad [3]$$

The F_m and F_g were calculated for a given temperature gradient ∇T of 100 K/mm and the results are shown in Figure 7. It can be seen that the Marangoni force is larger than the gravitational force when the Fe-rich sphere diameter is smaller than 425 μm. When the diameter of the Fe-rich sphere is within several microns, the Marangoni force is 10^2 to 10^3 times larger than the gravitational force. The microstructure of a $Cu_{60}Fe_{40}$ powder of 160-μm diameter is shown in Figure 8. It can be seen that the inner part (region A) of the powders shows a homogenous distribution of Fe-rich spheres, while the size of the Fe-rich spheres in region B is relatively large. The outer layer (region C) of the powder is almost free of Fe-rich spheres due to the spheres' Marangoni migration toward the center of the atomized droplet. The volume fraction of the Fe-rich sphere in the radius direction of the powder has been determined by the quantitative metallographic method and the results are shown in Figure 9. The volume fraction of the Fe-rich phase has a maximum in the region near the surface of the powder. The size distribution of the Fe-rich spheres in the $Cu_{60}Fe_{40}$ powder of 160-μm diameter has also been determined and the results are shown in Figure 10. The diameter of the Fe-rich spheres ranges from 0.22 to 4.56 μm. One can see by comparing Figures 5 and 10 that the size distribution of the Fe-rich

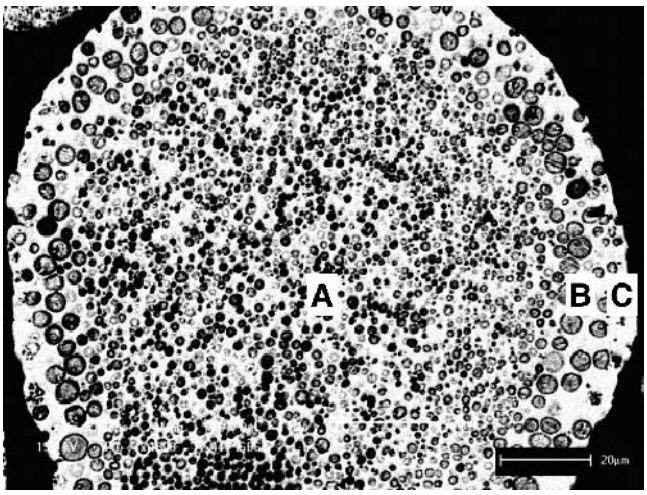

Fig. 8—The microstructure of a $Cu_{60}Fe_{40}$ powder of 160-μm diameter.

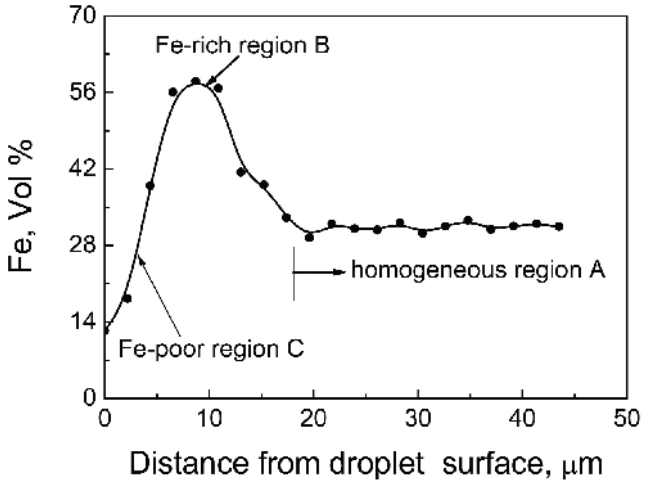

Fig. 9—Average volume fraction of Fe-rich spheres *vs* the distance from the surface of $Cu_{60}Fe_{40}$ powder of 160-μm diameter.

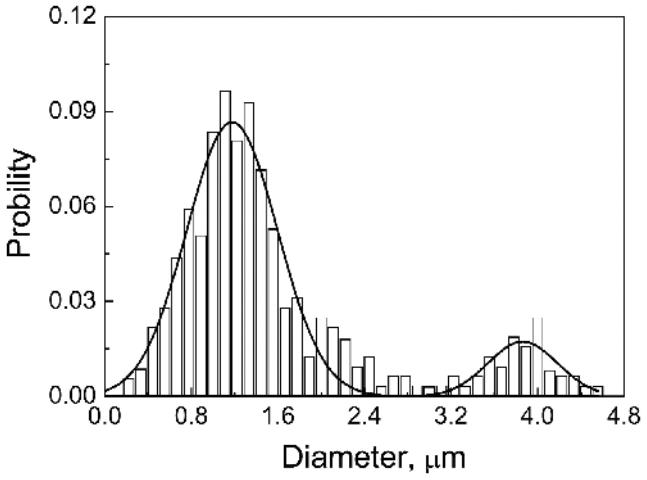

Fig. 10—The size distribution of Fe-rich spheres in the $Cu_{60}Fe_{40}$ powder of 160-μm diameter. The bars and solid curve are the measured and fitted results, respectively.

spheres in a larger powder is broader and even multipeak if the powder is large enough. This is the result of collisions and coagulations between the Fe-rich spheres due to their migration.[12]

D. *Interaction between the Sphere and Solidification Interface*

During cooling in the temperature interval range from T_{S_2} to T_{S_1}, there exist three possible interaction modes (pushing, engulfment, and entrapment) between the advancing solid/liquid interface and the Fe-rich sphere. The interaction modes relate to the interface morphology, i.e., planar, dendritic, cellular, and equiaxed.[17] Much work has been performed on the interaction between the foreign sphere and the solidification interface.[18] From the thermodynamic models, whether the sphere is pushed or engulfed by the solidification front was determined by thermophysical properties.[19] The thermodynamic models are presented as follows.

The thermal conductivity criterion:[20]

$$k_p/k_l < 1, \quad \text{for pushing} \qquad [4]$$

The heat diffusivity criterion:[21]

$$(k_p\rho_p C_p^p/k_l\rho_l C_p^l)^{1/2} < 1, \quad \text{for pushing} \qquad [5]$$

where k_p and k_l are the conductivity coefficients, ρ_p and ρ_l the densities, and C_p^p and C_p^l the specific heats of the Fe-rich sphere and the Cu-rich liquid matrix, respectively.[22,23,24]

The kinetic models were developed on the balance between a repulsive force and a dragging force, and the critical velocities for sphere engulfment were proposed in various models.[25] The kinetic model developed by Stefanescu *et al.*[26] is given by

$$V_c = \frac{1}{3\cdot\eta\cdot D}\left[\frac{\Delta\sigma\cdot a_0}{3}\left(2-\frac{k_p}{k_l}\right)\right] \qquad [6]$$

The model proposed by Shangguan *et al.*[27] is expressed as

$$V_c = \frac{2a_0k_l\Delta\sigma}{3\eta k_p(n-1)D}\left(\frac{n-1}{n}\right)^n \qquad [7]$$

where η is the viscosity, D is the diameter of the sphere, a_0 is the atomic diameter in the liquid, and $\Delta\sigma$ is the interfacial energy difference between the sphere-solid and sphere-liquid interfaces.

Judged from the thermodynamic models, the Fe-rich spheres are pushed by the advancing solid/liquid interface during the solidification of the Cu-rich matrix. The critical velocities for Fe-rich sphere engulfment, as predicted by the kinetic models, are given in Figure 11. The calculated critical velocity is in the range of 0.21 to 6×10^{-3} m s^{-1} for the Fe-rich spheres sized from 0.5 to 4.5 μm, as shown between two arrows in Figure 11. The growth rate of the Cu-rich grain is estimated to be 3 to 7×10^{-4} m s^{-1} according to the cooling rate in the atomization experiment, the released latent heat due to the crystallization of the Cu-rich matrix, and the grain size.[28,29] From the kinetic models, the Fe-rich spheres are also pushed by the advancing solid/liquid interface.

After the solidification of the Fe-rich sphere, the relative motion between the Fe-rich sphere and the Cu-rich phase matrix is almost negligible because the density difference

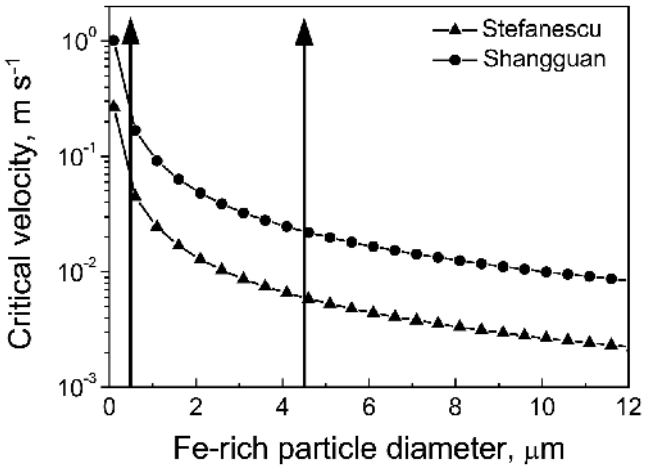

Fig. 11—The calculated critical interface velocities for sphere engulfment according to the models by Stefanescu *et al.*[26] and Shangguan *et al.*[27]

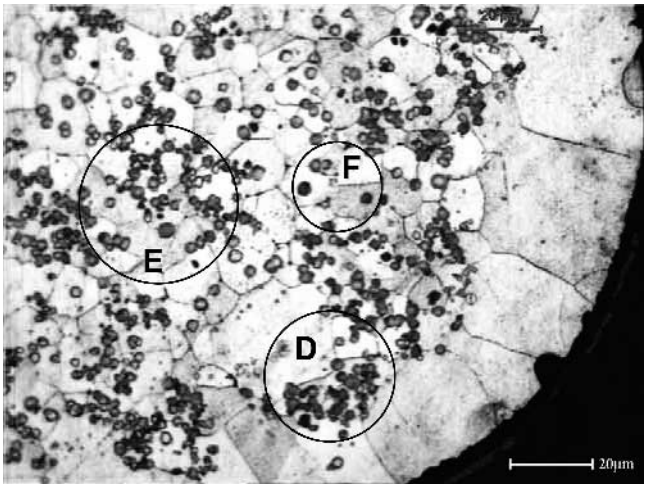

Fig. 12—The microstructure of a $Cu_{80}Fe_{20}$ alloy powder of 200-μm diameter.

between the Fe-rich sphere and the Cu-rich liquid phase is very small.[30] Once the solidification of the Cu-rich matrix starts from the surface of the atomized droplet, the Fe-rich spheres are pushed by the solidification interface. The microstructure of a $Cu_{80}Fe_{20}$ powder of 200-μm diameter is shown in Figure 12. The unidirectional solidification takes place and the cellular solidification interface is formed on the surface layer of the atomized droplet. The Fe-rich spheres are pushed by the advancing cellular interface, as illustrated in Figure 13(a). An Fe-poor layer is formed on the surface of the powder, and the Fe-rich spheres are piled in front of the cellular interface, as shown in region D of Figure 12, while in the center part of the atomized droplet, the equiaxed grains are produced due to the heat transfer in the free direction. The Fe-rich spheres are pushed by the equiaxed grain of the Cu-rich phase. The number density of the Fe-rich sphere near the equiaxed grains gradually increases with the growth of the grains, as shown schematically in Figure 13(b). As a result of the repulsive reaction between the Fe-rich sphere and the solid/liquid interface, Fe-rich spheres are entrapped between the grains, as indicated in Figure 13(c).

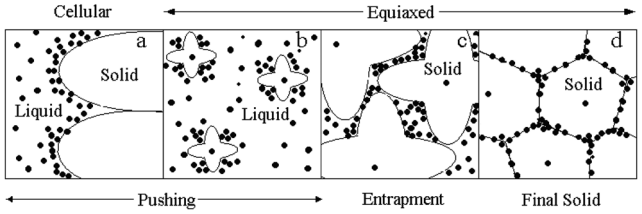

Fig. 13—Schematic illustration of the microstructure formation in the atomized droplet. (a) The Fe-rich spheres are pushed by the cellular solid/liquid interface. The Fe-rich spheres are (b) pushed and (c) entrapped by the equiaxed grains. (d) The solidification microstructure with most of the Fe-rich spheres distributed at the grain boundaries and triple junctions, and only a minority of Fe-rich spheres are embedded in the grain.

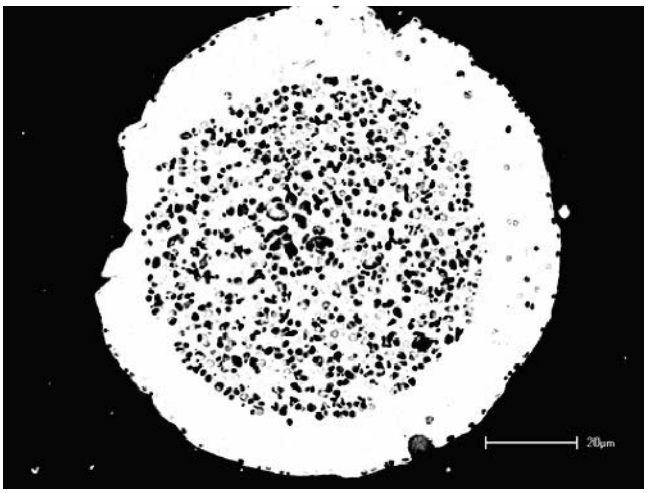

Fig. 14—The microstructure of a $Cu_{60}Fe_{40}$ alloy atomized powder of 120-μm diameter.

An alignment of the spheres along the grain boundaries results, and the entrapped spheres are eventually incorporated, as illustrated in Figure 13(d). Finally, most of the Fe-rich spheres locate at the grain boundaries and triple junctions, and a minority of the Fe-rich spheres are embedded in the grain near the boundaries (region E in Figure 12). The Fe-rich sphere embedded in the center of the grain may be the nucleus of the equiaxed grain of the Cu-rich phase (region F in Figure 12).

The microstructure of a powder with serious segregation of components is shown in Figure 14. Most of the Fe-rich spheres are segregated in the center region of the atomized droplet. On the surface layer of the powder, the formation of the Fe-poor layer is, according to the preceding analysis, attributed to two causes: one is the Fe-rich spheres' Marangoni migration toward the center of the atomized droplet, and the other is the pushing effect of the solidification interface on the Fe-rich spheres. The powder microstructure with the Fe-rich region encased by the Cu-rich phase resembles an egg. Recent research indicated that, if this microstructure consisted of an egg core that is high conductivity material and an egg white that is low melting point metal or alloy, the powders have great potential to be used as solder ball for modern electronics packaging technology.[31,32]

IV. CONCLUSIONS

The Cu-Fe alloys close to the critical composition are relatively easy to undercool into the metastable miscibility gap, and achieve a microstructure in which the minority phase is well dispersed in the form of spheres. The number density of the Fe-rich spheres increases while the average diameter of the minority phase spheres decreases with the decrease of the powder size. For a given-size powder, the average diameter of the Fe-rich spheres increases with the approach of the Fe content toward the critical composition. Under the gas atomization conditions, the Fe-rich spheres are pushed away by the solid/liquid interface. The formation of the Fe-poor layer on the powder surface is the common result of the Marangoni migration of the Fe-rich spheres during cooling in the metastable miscibility gap and the pushing effect of the advancing cellular solid/liquid interface on the Fe-rich spheres. The Fe-rich spheres in the center part of the powder are entrapped between the equiaxed grains of the Cu-rich phase and finally distribute at the grain boundaries and triple junctions.

ACKNOWLEDGMENTS

The authors gratefully acknowledge the financial support from the Sino-Germany Science Foundation (GZ032/1) and the National Natural Science Foundation of China (50271076, 50371092).

REFERENCES

1. L.J. Swartzendruber: in *Binary Alloy Phase Diagrams*, 2nd ed., T.B. Massalski, ed., ASME, New York, NY, 1990, pp. 1408-09.
2. Y. Nakagawa: *Acta Metall*., 1958, vol. 6, pp. 704-11.
3. Y.-Y. Chuang, R. Schmid, and Y.A. Chang: *Metall. Trans. A*, 1984, vol. 15 A, pp. 1921-30.
4. Q. Chen and Z.P. Jin: *Metall. Mater. Trans. A*, 1995, vol. 26A, pp. 417-26.
5. S.P. Elder, A. Munitz, and G.J. Abbaschian: *Mater. Sci. Forum*, 1989, vol. 50, pp. 137-50.
6. G. Wilde, R. Willnecker, R.N. Singh, and F. Sommer: *Z. Metallkd*., 1997, vol. 88, pp. 804-09.
7. G. Wilde and H.J. Perepezko: *Acta Mater*., 1999, vol. 47, pp. 3009-21.
8. A. Munitz: *Metall. Trans. B*, 1987, vol. 18B, pp. 565-75.
9. X.Y. Lu, C.D. Cao, and B. Wei: *Mater. Sci. Eng. A*, 2001, vol. 313A, pp. 198-206.
10. W.J. Yao, X.J. Han, and B. Wei: *Chin. Sci. Bull*., 2000, vol. 47, pp. 826-32.
11. G.E. Pellissier and S.M. Purdy: in *Stereology and Quantitative Metallography*, E.E. Underwood, ed., ASTM, New York, NY, 1979, pp. 1-30.
12. J.Z. Zhao, J.J. Guo, J. Jia, and Q.C. Li: *Trans. Nonferr. Met. Soc*., 1995, vol. 5, pp. 85-87.
13. N.O. Young, J.S. Goldstein, and M.J. Block: *J. Fluid Mech*., 1959, vol. 6, pp. 350-56.
14. M.G. Velarde: in *Materials and Fluid under Gravity*, L. Ratke, ed., Springer, Berlin, 1995, pp. 283-98.
15. W.R. Hu: *Microgravity Fluid Mechanics*, Science Press, Beijing, 1999, pp. 1-201.
16. J.W. Cahn and J.E. Hilliard: *J. Chem. Phys*., 1958, vol. 28, pp. 258-67.
17. F.R. Juretzko, B.K. Dhindaw, D.M. Stefanescu, S. Sen, and P.A. Curreri: *Metall. Mater. Trans. A*, 1998, vol. 29A, pp. 1691-6.
18. D.R. Uhlmann, B. Chalmers, and K.A. Jackson: *J. Appl. Phys*., 1964, vol. 35, pp. 2986-93.
19. D. Coupard, F. Girot, and J.M. Quenisset: *J. Mater. Sci*., 1996, vol. 31, pp. 5305-08.
20. A.M. Zubko, V.G. Lobanov, and V.V. Nikonova: *Sov. Phys. Crystallogr*., 1973, vol. 18, pp. 239-45.
21. M.K. Surappa and P.K. Rohatgi: *J. Mater. Sci. Lett*., 1981, vol. 16, pp. 765-69.
22. G. Pottlacher: *J. Non-Cryst. Solids*, 1999, vol. 251, pp. 177-81.
23. V.Y. Zinovyev, V.F. Polev, S.G. Taluts, G.P. Zinovyeva, and S.A. Ilinykh: *Phys. Met. Metall*., 1986, vol. 61, pp. 85-92.
24. V.YE. Zinovyev, S.G. Taluts, M.G. Kamashev, B.V. Vlasov, and V.P. Polyakova: *Phys. Met. Metall*., 1994, vol. 77, pp. 49-58.
25. R. Asthana and S.N. Tewari: *J. Mater. Sci*., 1993, vol. 28, pp. 5414-25.
26. D.M. Stefanescu, B.K. Dhindaw, S.A. Kacar, and A. Moitra: *Metall. Mater. Trans. A*, 1988, vol. 19A, pp. 2847-55.
27. D. Shangguan, S. Ahuja, and D.M. Stefanescu: *Metall. Trans. A*, 1992, vol. 23A, pp. 669-80.
28. W.D. Cai and E.J. Lavernia: *Metall. Mater. Trans. B*, 1998, vol. 29B, pp. 1085-96.
29. T. Suzuki, S. Toyoda, T. Umeda, and Y. Kimara: *J. Cryst. Growth*, 1977, vol. 38, pp. 123-28.
30. T. Tanaka, K. Hack, T. Iida, and S. Hara: *Z. Metallkd*., 1996, vol. 87, pp. 380-89.
31. X.J. Liu, I. Ohnuma, C.P. Wang, M. Jiang, R. Kainuma, K. Ishida, M. Ode, T. Koyama, H. Onodera, and T. Suzuki: *J. Electron. Mater*., 2003, vol. 32, pp. 1265-72.
32. C.P. Wang, X.J. Liu, I. Ohnuma, R. Kainuma, and K. Ishida: *Science*, 2002, vol. 297, pp. 990-93.